ACS APPLIED POLYMER MATERIALS

pubs.acs.org/acsapm

Article

Reactive Molecular Dynamics Simulation of Epoxy for the Full Cross-Linking Process

Sagar Umesh Patil, Sagar P. Shah, Michael Olaya, Prathamesh Prashant Deshpande, Marianna Maiaru, and Gregory M. Odegard*

Cite This: *ACS Appl. Polym. Mater.* 2021, 3, 5788–5797

Read Online

ACCESS | Metrics & More | Article Recommendations | Supporting Information

ABSTRACT: Epoxy resins are used extensively in composite materials for a wide range of engineering applications, including structural components of aircraft and spacecraft. The processing of fiber-reinforced epoxy composite structures requires carefully selected heating and cooling cycles to fully cure the resin and form strong cross-linked networks. To fully optimize the processing parameters for effective epoxy monomer cross-linking and final product integrity, the evolution of mechanical properties of epoxies during processing must be comprehensively understood. Because the full experimental characterization of these properties as a function of degree of cure is difficult and time-consuming, efficient computational predictive tools are needed. The objective of this research is to develop an experimentally validated Molecular Dynamics (MD) modeling method, which incorporates a reactive force field, to accurately predict the thermo-mechanical properties of an epoxy resin as a function of the degree of cure. Experimental rheometric and mechanical testing are used to validate an MD model, which is subsequently used to predict mass density, shrinkage, elastic properties, and yield strength as a function of the degree of cure. The results indicate that each of the physical and mechanical properties evolve uniquely during the cross-linking process. These results are important for future processing modeling efforts.

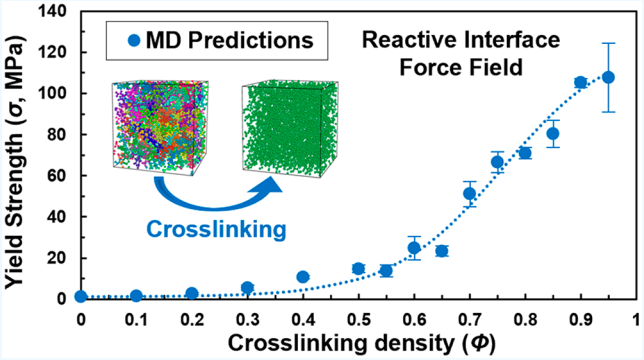

KEYWORDS: *computational simulation, materials genome, ICME, strain-rate, process modeling, IFF-R, interface force field*

1. INTRODUCTION

Thermosetting epoxies are an excellent candidate to be utilized for a variety of applications in the aerospace industry. They possess excellent mechanical, thermal, and electrical properties.[1] In addition, epoxies are widely used for benchmarking research as they are inexpensive, and epoxy-based composites are relatively easy to fabricate following simple curing protocols.[2] During the curing of composite panels, the epoxy matrix is subjected to elevated temperatures, and the corresponding thermo-mechanical properties evolve as the curing progresses. Additionally, the epoxy matrix experiences shrinkage during the cure process. Because the evolving matrix thermo-mechanical properties and shrinkage drive the development of residual stresses in composite panels during the curing process, a better understanding of the evolution of these properties is important for optimizing the composite processing parameters. The full experimental characterization of composite property/shrinkage evolution is time-consuming and expensive.

Molecular dynamics (MD) is a powerful tool to simulate molecular behavior and provide insight into the effect of temperature, pressure, and other design parameters on the complex networked molecular structure that epoxies possess.[3,4] As a result, these simulations can also provide atomistically informed predictions of the evolution of thermo-mechanical properties and the shrinkage of epoxy during processing. All MD techniques utilize a force field to describe the interaction of bonded and nonbonded atoms in the molecule. The correct choice of force field based on the design objectives is necessary to accurately simulate the molecular behavior and predict accurate properties.[5,6]

For decades, MD simulations of polymer-based engineering materials have been mostly limited to using fixed-bond force fields with harmonic bonds, that is, force fields that do not simulate the formation or scission of covalent bonds. Specifically, MD modeling studies[3] for neat epoxies have employed various fixed-bond force fields such as OPLS-UA,[7,8] CHARM and cff91,[9] CVFF,[10,11] PCFF,[12] Dreiding,[13−18] COMPASS,[19−22] AMBER,[23] and MMFF.[24] Reactive force

Received: August 14, 2021
Accepted: September 28, 2021
Published: October 12, 2021

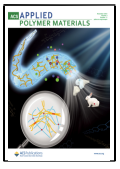

fields allow for the direct simulation of the formation and/or scission of covalent bonds during the simulated deformation process, thus allowing for accurate predictions of strength and mechanical properties at large deformations. In particular, the reactive force field ReaxFF has been used to simulate epoxy systems and accurately predict mechanical properties.[25−27] However, ReaxFF is highly complex; thus MD simulation times utilizing this force field are prohibitively long and limited to relatively small simulations.

Recently, Winetrout et al.[28] developed the Reactive Interface Force Field (IFF-R), which combines the efficiency of a fixed-bond Interface force field (IFF)[29] with the capability of simulating bond scission. IFF-R replaces the traditional harmonic bond-stretching potential with a morse potential to model covalent bond dissociation in response to large local mechanical deformations. Pisani et al.[30] used IFF-R to simulate polyamide nanocomposites, and Odegard et al.[31] demonstrated the capability of IFF-R for accurately predicting mechanical properties of fully cured epoxy systems. However, IFF-R has not yet been used to simulate partially cured epoxy systems.

All of the MD modeling studies of epoxy cited above provide predicted properties for either a fully cured epoxy or a semicured epoxy at a limited number of intermediate cross-linking densities. None of these studies provide predicted properties for a large range of cross-link densities, which is necessary for comprehensive, multiscale process modeling methods for optimizing thermo-mechanical properties of epoxy composites and minimizing process-induced residual stresses.[32−37] Further, the accuracy of predicted mechanical properties using MD is highly dependent on the accurate prediction of the mass density, which represents the bulk density of the polymer.[24] All of the MD studies discussed above that employ fixed-bond force fields show a significant discrepancy between their MD predicted mass density and the experimentally measured bulk density of the respective material. This discrepancy manifests in the inaccurate prediction of mechanical properties, which adversely affects the prediction of residual stresses in a multiscale process modeling framework. The above-cited studies that utilize ReaxFF demonstrate accurate prediction of mass density but do so at the expense of model size and efficiency.

This work utilizes MD simulation to accurately predict the physical and mechanical properties of an epoxy system at varying degrees of cure ranging from fully uncross-linked to fully cross-linked states at room temperature (300 K, 27 °C). This study implements IFF-R to accurately predict the physical and mechanical properties corresponding to large deformations. The modeling approach is validated herein using experimental characterization of the epoxy system. The results of this study provide the input necessary for comprehensive process modeling of epoxy composites and key insight into the gelation process of epoxy during curing.

2. MOLECULAR MODELING

2.1. Material System and Force Field. For this study, an epoxy system comprised of diglycidyl ether bisphenol F (DGEBF) resin and diethyltoluenediamine (DETDA) hardener was modeled using the IFF-R force field. Figure 1 shows the molecular structures of both monomers. The LAMMPS[38] (Large-scale Atomic/Molecular Massively Parallel Simulator) software package was used to perform all of the MD simulations for this work. The properties predicted are the bulk mass density (ρ), post-gelation volumetric shrinkage, bulk

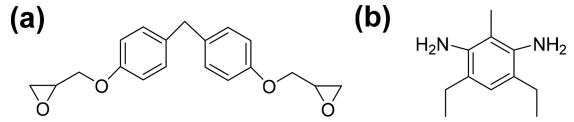

Figure 1. Molecular structures of (a) DGEBF (EPON 862) resin and (b) DETDA (Epikure W) hardener.

modulus (K), shear modulus (G), Young's modulus (E), Poisson's ratio (ν), and yield strength (σ). The energy terms associated with IFF-R and ReaxFF are described in the Supporting Information.

2.2. Model Setup. For the first step in the MD modeling procedure, a series of equilibrated MD models were constructed. First, both of the monomers were assigned IFF-R parameters and combined in a large orthogonal simulation box with a resin-to-hardener ratio of 2:1. The system was replicated to produce 90 monomers of DGEBF and 45 monomers of DETDA to create a low-density MD model containing 5265 atoms. To allow the monomers to mix, a fixed-volume and fixed-temperature (NVT) simulation was performed over 100 ps (ps) with 1 fs (fs) time steps at 600 K. Following this mixing simulation, the simulation box was slowly compressed (densified) to a target density of 1.17 g/cm^3. This simulation occurred at 300 K over 8 ns (ns) at 1 fs time steps. After densification, an annealing simulation was performed, during which the temperature was ramped from 300 to 600 K and then slowly cooled to 300 K at a 20 K/ns cooling rate with the NVT ensemble. A fixed-pressure and fixed-temperature (NPT) simulation was performed at 300 K and 1 atm for 1 ns with 1 fs timesteps to allow the atoms to reconfigure and attain stable energy positions. Shown in Figure 2 is a representative image of the fully densified and

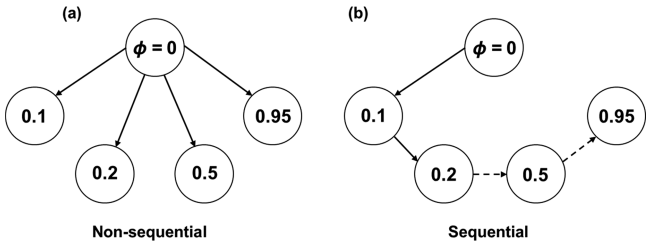

Figure 2. Cross-linking strategies: (a) nonsequential and (b) sequential.

equilibrated structure. By repeating this procedure, five different replicates were created to account for statistical deviations in predicted properties. The Nose−Hoover thermostat and barostat were implemented for all of the simulations discussed herein.[39−41] Once all five replicates were annealed and relaxed, the next step was cross-linking.

2.3. Cross-Linking of Epoxy Monomers. The DGEBF/DETDA epoxy system follows a two-step cross-linking reaction.[42] In the first step, the epoxide ring of one DGEBF monomer opens, and the exposed epoxide carbon reacts with a nitrogen from a primary amine (−NH_2) of DETDA and forms a hydroxyl group and a secondary amine (−NH). In the second step, the newly formed secondary amine reacts with the epoxide carbon of another DGEBF monomer to form a tertiary amine (−N) and a second hydroxyl group. The "fix bond/react" command developed by Gissinger et al.[43] in LAMMPS was implemented to simulate these reactions. This command allows for the simulation of user-defined cross-links. The

https://doi.org/10.1021/acsapm.1c01024
ACS Appl. Polym. Mater. 2021, 3, 5788−5797

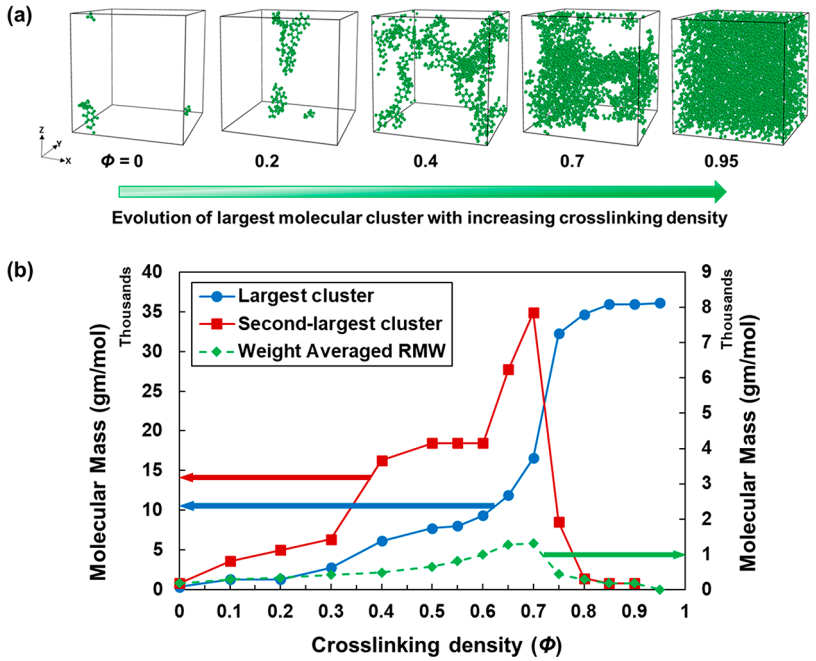

Figure 3. (a) Snapshots of the largest cluster and (b) molecular mass as a function of varying cross-linking densities for a representative system.

required prereaction, postreaction, and mapping templates were created accordingly. These simulations were performed at 450 K with 0.1 fs timesteps. Individual models with cross-linking densities varying from 0 to 0.95 were created for all five replicates. Here, the cross-linking density (ϕ) is defined as the ratio of the number of cross-links formed to the maximum possible cross-links that could be formed in the entire system. A video showing the covalent bond breaking and formation between two DGEBF monomers and one DETDA hardener is included in the Supporting Information. The video is rendered using OVITO[44] visualization software. During these simulations, the density and volume of the simulation boxes were tracked. Following the cross-linking, an NPT simulation was performed for each cross-linking density at 300 K for 1 ns at 1 fs timesteps to relax the model and to predict the final density and volume. The volumetric shrinkage was calculated as the percent change in the volume of the cross-linked model at specific cross-linking densities, with respect to the uncross-linked model. For all simulations, the Nose−Hoover barostat was set to maintain a 0.101 MPa (1 atm) pressure on all sides of the simulation box.

Two cross-linking strategies were investigated as shown in Figure 2. For the nonsequential approach, each cross-linked model was generated starting from the same uncross-linked (ϕ = 0) model. That is, cross-linking steps were performed directly from 0 to 0.1, 0 to 0.2, and so on, up to the last step, 0 to 0.95. For the sequential approach, each cross-link density was achieved from the increment before it. That is, cross-linking was performed from 0 to 0.1, then 0.1 to 0.2, and so on up until the final increment of 0.9 to 0.95. The progressive building of cross-links in the sequential strategy mimics the actual curing of polymers and hence was adopted for this study. In addition, a comparison of properties such as mass density, post-gelation volumetric shrinkage, and bulk modulus predicted from both strategies is included in the Supporting Information. For both of the strategies, a cross-linked MD model was built individually for each cross-linking density at 450 K and was cooled to 300 K. Afterward, an NPT simulation at 300 K and 1 atm was run for 1 ns to relax the models and allow the cross-linked molecules to attain minimum energy states.

2.4. Gel Point Prediction. According to Flory,[45] an infinite network is formed at the polymer gel point where a single molecule is large enough to span the entire length of the system. Here, the largest molecule represents the largest cluster (group of connected polymer units) in the simulation box. Figure 3a shows the growth of the largest cluster as a function of varying cross-linking density for a representative system. The gel point can be predicted via MD simulation by tracking the molecular weight of the largest cluster, the molecular weight of the second-largest cluster, or the weight-averaged reduced molecular weight (RMW) of the system.[10,46,47] The RMW is the molecular weight of the entire system except for the largest cluster. When the largest cluster metric is used, the inflection point at which the largest cluster molecular weight drastically increases marks the gel point. When the other two metrics are used, the gel point occurs at the point where the corresponding molecular weight reaches a peak value.

In this work, the gel point was predicted using all three methods. Figure 3b shows the representative results for all three metrics for one replicate. The average gel points of the five replicates were 0.63, 0.60, and 0.62 for the largest cluster, second-largest cluster, and RMW metrics, respectively. These values agree well with other modeling results from the literature for the same epoxy sytem.[10,46,47] Figure 7 shows representative snapshots of the largest cluster at different cross-linking densities, demonstrating the evolution of an infinite network in a periodic simulation box. The "Cluster analysis" modifier in the OVITO[44] visualization software was implemented to generate these images. When the cross-linking begins, the simulation box contains only monomers. As the cross-linking progresses, covalent bonds form between the monomers and the network starts to grow. In Figure 7, at 0.2 cross-linking density, the network formation initiates. At a cross-link density of 0.4, the network is not yet large enough to span the entire simulation box. Finally, at 0.7 the largest cluster

https://doi.org/10.1021/acsapm.1c01024
ACS Appl. Polym. Mater. 2021, 3, 5788−5797

spans the simulation box, which indicates that a continuous load-carrying covalent bond network exists in each direction, and the polymer has reached the gel point. The gel point generally varies between replicates and is highly dependent on the starting molecular configuration. The value of $\phi = 0.6$ was chosen as the gel point of this system for calculation of the post-gelation volumetric shrinkage because it is the simulated value that is closest to the average gel points predicted using all three metrics.

2.5. Mechanical Deformation Simulations. The next step in the analysis was to perform simulated mechanical deformations. Here, K, G, E, ν, and σ for each cross-linking density for all replicates were predicted by implementing the simulation procedures similar to those outlined by Odegard et al.[31] For each replicate and cross-link density, K was predicted from 1 and 5000 atm NPT simulations at 300 K, and G was determined from shear deformations in the three principal planes. The (K,G) pair was then used to predict the (E,ν) pair using the standard relations for linear elastic isotropic materials.[48] The yield strength was predicted using the von Mises stress calculated from the shear deformations.[31] A detailed description of the procedure and necessary equations implemented in this work to predict the mechanical properties using the MD simulation results is included in the Supporting Information.

3. EXPERIMENTAL DETAILS

The experimental procedure for the measurement of the mass density is described by Odegard et al.[31] This section describes the measurement of gel point, volumetric shrinkage, and mechanical properties for the DGEBF/DETDA epoxy.

3.1. Specimen Preparation. The DGEBF/DETDA epoxy resin system components were first measured according to a stoichiometric ratio of 100:26.4 (parts by weight) and then mixed thoroughly by hand for 2 min at room temperature. Significant air entrainment as a result of the mixing process was observed. To eliminate the trapped air, the uncured resin mixture was first heated in an oven held at 80 °C for 20 min, and then degassed at room temperature for an additional 20 min. The heating step served as a means to reduce the resin viscosity for a more effective degassing procedure. For the gel point and volumetric shrinkage characterization described below, the degassed mixture was directly tested in this state. For the mechanical characterization, the degassed mixture was injected into an open-faced mold for full curing of tensile test specimens. The specimens were manufactured according to ASTM D638 Type I specifications. Once fully cured and cooled to room temperature, each specimen was water-polished to eliminate any irregularities found in the cross-sectional area along the gage length of the specimen as a result of curing in open-faced molds. After being polished, a black/white contrasting speckle pattern was applied to the specimens in preparation for 2-D Digital Image Correlation (DIC) strain measurement[49,50] during tensile testing.

3.2. Gel Point and Volumetric Shrinkage Testing. To experimentally evaluate the gel point and the post-gelation chemical shrinkage (ε_{sh}) of the DGEBF/DETDA epoxy, a rotational rheometer (ARES-G2, TA Instruments) with a parallel plate setup was used. The resin mixture, prepared following the aforementioned procedure, was injected between the parallel plates, which had an initial gap $h_0 = 1.5 \pm 0.05$ mm. The mixture was then rapidly heated to the desired temperature and allowed to soak under isothermal conditions. For this study, the tests were conducted at two isothermal temperatures of 150 and 170 °C.

Gel point measurements were carried out in gap-control mode. As the resin mixture cured, it was subjected to an oscillating shear strain, which induced a shear stress in the curing resin. The complex shear modulus G, decomposed into its elastic storage shear modulus G' and viscous loss shear modulus G'', was measured by the rheometer. The point during the cure process at which both G' and G'' intersect (have equal values) indicates the transition of the material from a primarily liquid/viscous to solid/elastic phase. This point was used to determine the time to gelation.[51] Considering the time−temperature history of the rheology test, the degree of cure corresponding to the gel time was calculated from the kinetic model for DGEBF/DETDA.[52] An average gel point, across four tests performed at the two different isothermal temperatures, was found to be 0.71, which is in excellent agreement with experimental data found in the literature for the DGEBF/DETDA[51] epoxy system.

Evaluation of post-gelation volumetric shrinkage (ε_{sh}) was performed with the same rheometer setup as the gel point measurement. To measure post-gelation chemical shrinkage (as determined above), the instrument was operated in force-control mode during which a normal force of 0.1 N was applied to maintain contact between the shrinking specimen and the plates. The linear variation $(h - h_0)$ in the gap h resulting from the chemical shrinkage in the specimen was continuously monitored by the instrument. The ε_{sh} resulting from the cure was computed using

$$\varepsilon_{sh} = \left[1 + \frac{1}{3}\left(\frac{h - h_0}{h_0}\right)\right]^3 - 1 \quad (1)$$

This relationship assumes that there are no in-plane strains in the specimen and the material is incompressible ($\nu = 0.5$). The average post-gelation volumetric shrinkage in the fully cured specimens was $2.36 \pm 0.08\%$. With the knowledge of the time−temperature history of the test, the degree of cure was computed using the kinetic model described elsewhere.[52] Figures showing the measured post-gelation volumetric shrinkage as a function of time and degree of cure are included in the Supporting Information.

3.3. Mechanical Testing. The tensile test specimens were tested according to ASTM D638 guidelines to determine the tensile stiffness, Poisson's ratio, and 0.2% offset yield strength. Each specimen was subjected to a uniaxial tensile load using an MTS model 43.104 electromechanical test machine in displacement control mode with a crosshead displacement rate of 2 mm/min. During specimen deformation, photographs were captured at even intervals throughout the test up to the point of fracture. A FUJIFILM X-T3 26.1-megapixel camera was utilized for acquiring the photographs.

The open-sourced DIC platform Ncorr[49,50] built within Matlab was used for the DIC analyses after tensile testing was completed. In performing DIC analyses, deformations of the patterned specimens under loading were measured relative to a reference (undeformed) image through image recognition algorithms.[49] As a result, axial and transverse full-field strains within a user-specified region of interest (ROI) were calculated for each photograph taken during a given test. In this characterization procedure, the full-field strains were averaged for each photograph and then correlated to the corresponding time, load, and displacement readings provided by the MTS apparatus. The ROI was selected to be within the gage area as specified elsewhere.[53] Postprocessed data were in the form of stress−strain curves, one for each test specimen.

The characterization of the modulus, Poisson's ratio, and offset yield strength was performed using only data from tests in which the specimen fractured within the gage area as designated by ASTM D638. Young's modulus was calculated by performing a fit of the initial linear region of the stress−strain curve up to 1% strain. Poisson's ratio was determined by taking a linear fit of the negative of the strains in the transverse direction divided by the strains in the axial direction. The yield strength was measured as the stress corresponding to the strain 0.2% offset from a deviation of the proportional limit of the stress−strain curve. The strain-rate was estimated by calculating the average of the slope of adjacent strain-time data points.

4. RESULTS

This section describes the results of the MD simulations. For each of the plots provided in this section, the black dots

https://doi.org/10.1021/acsapm.1c01024
ACS Appl. Polym. Mater. 2021, 3, 5788−5797

represent MD predictions, and the error bars represent the standard error associated with the predictions of the replicate models. All curve fits to the MD data shown in this section were performed using equations that best matched the form of the data using OriginPro[54] data analysis software. The MD predicted properties for the fully cross-linked model (ϕ = 0.95) are compared to the experimentally measured values from the current work and from the literature.

4.1. Mass Density. Figure 4 shows the mass density as a function of cross-linking density at room temperature. The

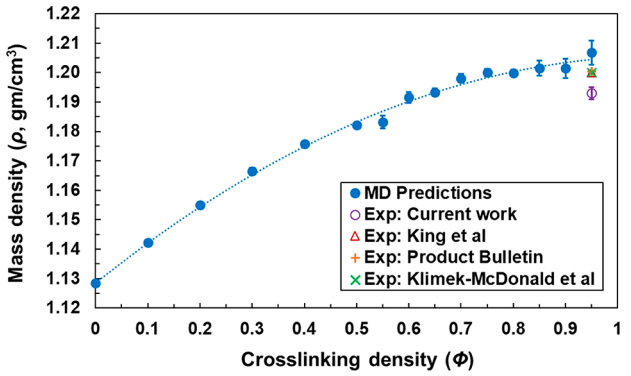

Figure 4. Predicted mass density as a function of cross-linking density at room temperature.

predicted mass density at 300 K for the fully cross-linked system (ϕ = 0.95) is found to be 1.207 ± 0.003 g/cm^3. This value agrees well with the experimentally measured value of 1.193 g/cm^3 for fully cured DGEBF/DETDA epoxy in this work. The MD prediction at ϕ = 0.95 is also compared to the experimental value of 1.20 g/cm^3 from the literature.[55−57] The mass density gradually increases with increasing cross-linking density. This can be attributed to increased network connectivity due to the formation of covalent bonds between the monomers, which reduces the distance between monomers and thus increases the mass density. It can also be seen from Figure 4 that the MD predicted mass density for the fully cross-linked system agrees well with the experimental data from the literature and from this work. It is also noteworthy that the literature values show closer agreement with the predictions than do the experimental values from this work. This suggests that there is a wide range of experimental values due to differences in the sample preparation procedures and mass density measurement techniques. The mass density data were fitted with a second-order polynomial with R^2 = 0.998 as defined by

$$\rho\left(\frac{\mathrm{g}}{\mathrm{cm}^3}\right) = -0.065 \times \phi^2 + 0.142 \times \phi + 1.128 \quad (2)$$

4.2. Volumetric Shrinkage. Figure 5 shows the total volumetric shrinkage as a function of cross-linking density at room temperature. The predicted shrinkage for the fully cross-linked system (ϕ = 0.95) is 6.496 ± 0.184%. This agrees well with the shrinkage observed during the experimental curing of epoxy resins.[3] The volumetric shrinkage gradually increases with increases in the cross-linking density because of the formation of covalent bonds. The MD data were fitted using a second-order polynomial with R^2 = 0.994 showing a nonlinear dependence between volumetric shrinkage and cross-linking density as defined by

$$\text{volume shrinkage (\%)} = -5.806 \times \phi^2 + 12.146 \times \phi + 0.044 \quad (3)$$

A similar nonlinear trend was observed for this epoxy system using the Dreiding force field.[17]

The inset in Figure 5 shows the post-gelation volumetric shrinkage, which is calculated as the change in volume of the cross-linked model with respect to the volume of the model at ϕ = 0.6 at the onset of gelation. The MD predicted post-gelation volumetric shrinkage at ϕ = 0.95 is 1.543 ± 0.417% at room temperature. This value agrees well with the experimentally measured value of 2.36 ± 0.08% in this work. The MD data were fitted using a linear curve fit with R^2 = 0.912 showing a linear dependence between post-gelation volumetric shrinkage and cross-linking density as defined by

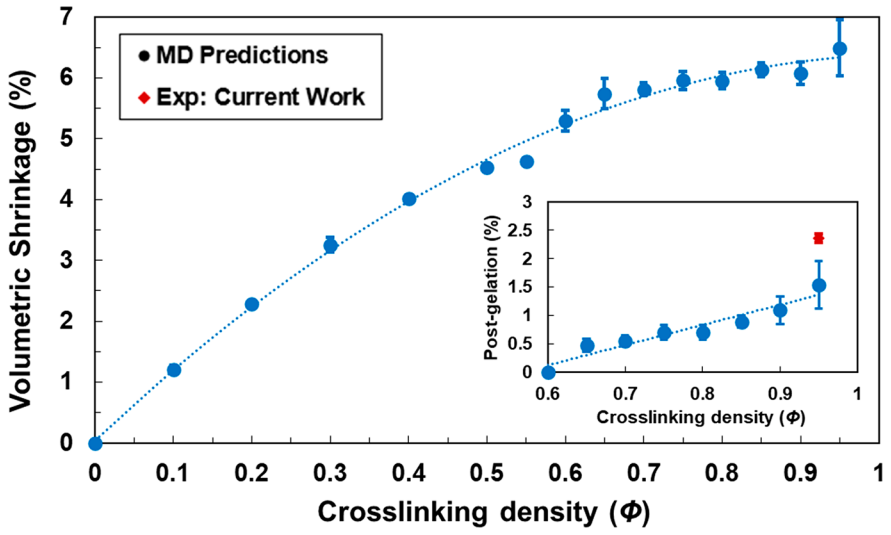

Figure 5. Predicted volumetric shrinkage as a function of cross-linking density at room temperature. Post-gelation volumetric shrinkage as a function of cross-linking density at room temperature (inset).

https://doi.org/10.1021/acsapm.1c01024
ACS Appl. Polym. Mater. 2021, 3, 5788−5797

post-gelation volumetric shrinkage (%)

$$= 3.545 \times \phi - 2.003 \quad (4)$$

This linear dependence between post-gelation shrinkage and cross-linking density is in general agreement with the experimentally observed linear dependence between post-gelation shrinkage and degree of cure as shown in the Supporting Information.

4.3. Bulk Modulus. Figure 6 shows the predicted bulk modulus as a function of the cross-linking density. A bulk modulus of 5.546 ± 0.107 GPa was predicted for the fully cross-linked system (ϕ = 0.95). The bulk modulus gradually increases with cross-linking density, and as it reaches gelation at ϕ = 0.6, the value approaches a constant value as the material transforms to a solid phase after gelation. Because it is difficult to measure K experimentally, MD predictions are an efficient means of determining this at varying cross-linking densities. The MD data in Figure 6 were fitted with a quadratic curve fit with R^2 = 0.986 showing a nonlinear dependence between K and cross-linking density as defined by

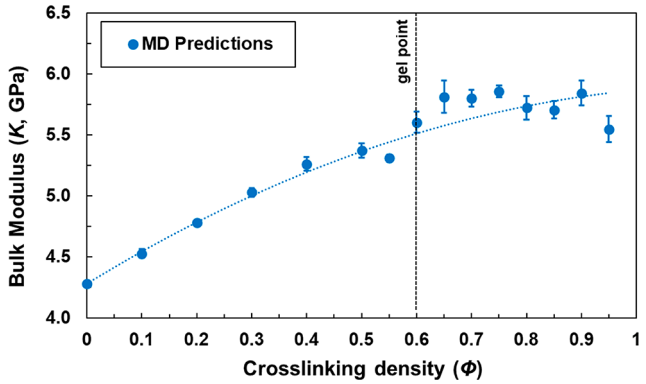

Figure 6. Predicted bulk modulus as a function of cross-linking density at room temperature.

$$K\ (\text{GPa}) = -1.157 \times \phi^2 + 2.743 \times \phi + 4.283 \quad (5)$$

4.4. Shear Modulus. Figure 7 shows the predicted shear modulus as a function of cross-linking density. A shear modulus of 1.222 ± 0.267 GPa was predicted for ϕ = 0.95. This value is compared to the experimentally measured values at three different strain-rates from Littell et al.[58] The variation between MD predictions and experimental measurements is due to the orders-of-magnitude difference in strain-rates.[27] The shear modulus for the uncross-linked epoxy is a finite value also because of the strain-rate effect.[27] Because of the unavailability of experimental data for intermediate cross-linking densities in the literature, the comparison with MD predictions was not made here for shear modulus, Young's modulus, Poisson's ratio, and yield strength. However, the comparison with the maximum cross-linking density (ϕ = 0.95) qualitatively validates the predictions for all other values as the same procedure was followed to predict the properties for the entire range of cross-linking densities. The MD data in Figure 7 were fitted with a linear curve fit with R^2 = 0.984 showing a linear dependence between G and cross-linking density as defined by

$$G\ (\text{GPa}) = 0.969 \times \phi + 0.154 \quad (6)$$

4.5. Young's Modulus. Figure 8 shows the predicted Young's modulus as a function of cross-linking density. E = 3.407 ± 0.701 GPa was predicted for ϕ = 0.95. Also shown in the figure are the experimentally measured values at different strain-rates.[58,59] The experimentally measured value of 2.230 GPa at 2.22 × 10^{-4} s^{-1} strain-rate in this work agrees well with the other experimental data from literature. Despite the strain-rate difference between MD simulations and experiments, the predictions at ϕ = 0.95 match well with the higher strain-rate (7 × 10^2 s^{-1}) experimental data from the Split-Hopkinson Bar test of Gilat et al.[59] (results analyzed by Odegard et al.[31]). Overall, the Young's modulus gradually increases with increasing cross-linking density. This gradual increase is due to the increased network connectivity, which makes the material stiffer and able to sustain load. No significant change in the magnitude can be seen in the predictions above ϕ = 0.7, as the material attains gelation. The MD data in Figure 8 were fitted with a linear curve fit with R^2 = 0.985 showing a linear dependence between E and cross-linking density as defined by

$$E\ (\text{GPa}) = 2.732 \times \phi + 0.461 \quad (7)$$

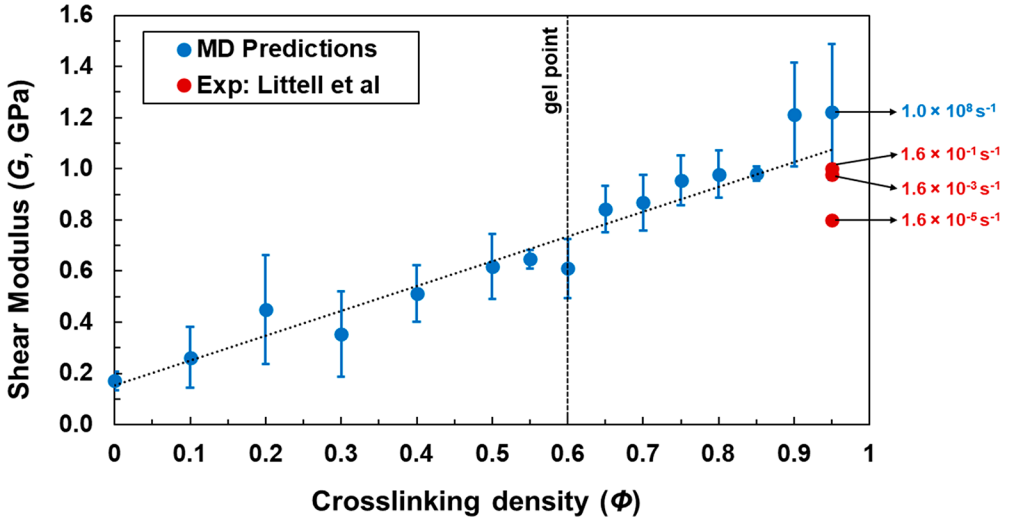

Figure 7. Predicted shear modulus as a function of cross-linking density at room temperature. Callouts refer to the corresponding strain-rate.

https://doi.org/10.1021/acsapm.1c01024
ACS Appl. Polym. Mater. 2021, 3, 5788−5797

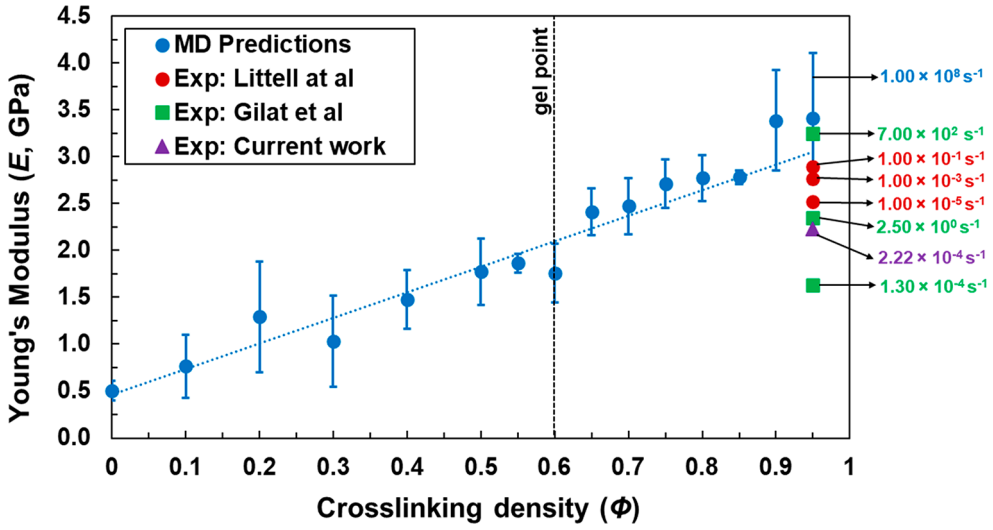

Figure 8. Predicted Young's modulus as a function of cross-linking density at room temperature. Callouts refer to the corresponding strain-rate.

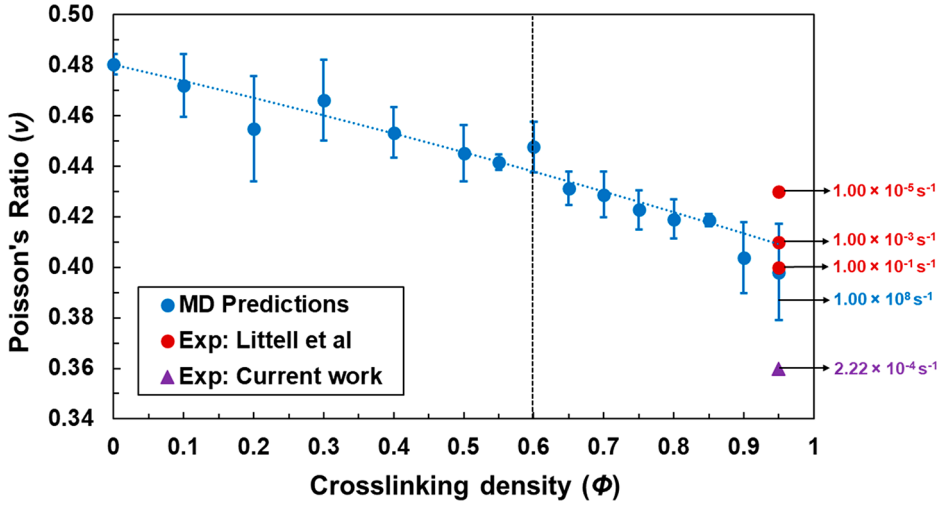

Figure 9. Predicted Poisson's ratio as a function of cross-linking density at room temperature. Callouts refer to the corresponding strain-rate.

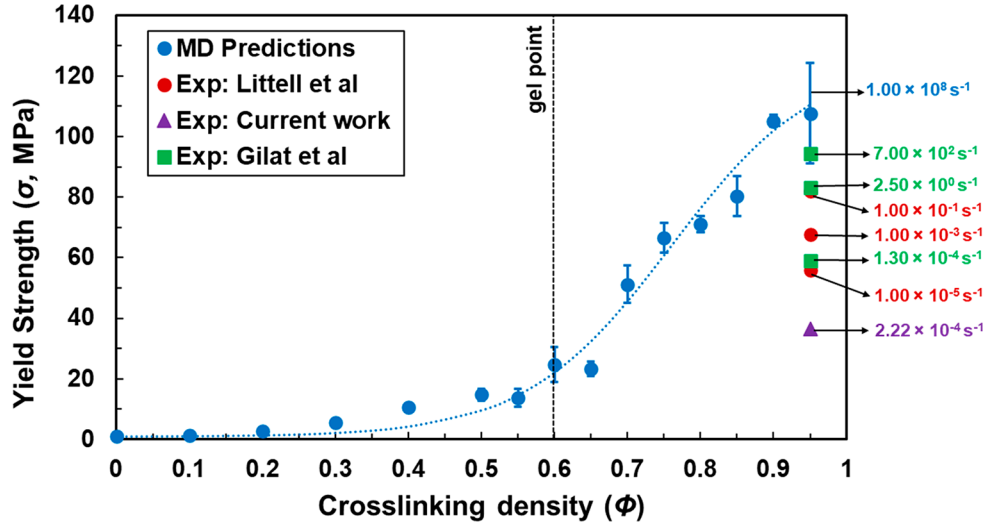

Figure 10. Predicted yield strength as a function of cross-linking density at room temperature. Callouts refer to the corresponding strain-rate.

4.6. Poisson's Ratio. Figure 9 shows the predicted Poisson's ratio as a function of cross-linking density. A Poisson's ratio of 0.398 ± 0.019 was predicted for $\phi = 0.95$ and of 0.480 ± 0.004 was predicted for $\phi = 0$. Also shown in the

https://doi.org/10.1021/acsapm.1c01024
ACS Appl. Polym. Mater. 2021, 3, 5788−5797

figure are the experimentally measured values at different strain-rates from Littell et al.[58] The experimentally measured value of 0.360 at a 2.22×10^{-4} s^{-1} strain-rate in this work agrees well with the data from the literature. The Poisson's ratio gradually decreases with increasing cross-linking density. The MD predictions at $\phi = 0.95$ agree well with the experimental values despite the difference in strain-rates, which demonstrates a smaller influence of the strain-rate on the Poisson's ratio relative to the Young's modulus and shear modulus. It can also be seen from Figure 9 that the MD predicted Poisson's ratio for the fully cross-linked system agrees well with the experimental data from this work and the literature. The better agreement of the literature values suggests that there is a substantial amount of variability in the Poisson's ratio given different specimen preparation and testing techniques, and more measurement sampling could improve the agreement with the predictions. The MD data in Figure 9 were fitted with a quadratic curve fit with $R^2 = 0.985$ showing a nonlinear dependence between ν and cross-linking density as defined by

$$\nu = -0.012 \times \phi^2 - 0.063 \times \phi + 0.480 \quad (8)$$

4.7. Yield Strength. Figure 10 shows the predicted yield strength as a function of cross-linking density. A yield strength of 107.67 ± 16.67 MPa was predicted for $\phi = 0.95$. In the figure, this value is compared to the experimentally measured values at different strain-rates.[58,59] The experimentally measured value of 36.54 MPa at a 2.22×10^{-4} s^{-1} strain-rate in this work agrees well with the experimental data from the literature. It can also be seen in Figure 10 that at $\phi = 0.95$ the yield strength increases with increasing strain-rate, and the experimental value at the highest strain-rate from Gilat et al.[59] (as was analyzed by Odegard et al.[31]) matches well with the MD prediction. The yield strength increases with increasing cross-linking density due to increased network connectivity. In the pre-gelation regime ($\phi = 0$–0.6) the yield strength is low, as the material is a viscous liquid and cannot sustain large mechanical loads. The yield strength value increases quickly as the material reaches gelation ($\phi = 0.6$) and continues to increase in the post-gelation regime ($\phi = 0.6$–0.95) as the material attains a tighter network and can sustain significant loads. The MD data are fitted with a sigmoidal (Boltzmann equation) curve fit with $R^2 = 0.885$, which correctly represents the evolution of the yield strength of the epoxy from the uncross-linked liquid phase to the fully cross-linked solid phase as defined by

$$\sigma\ (\text{MPa}) = 123.839 + \frac{(0.983 - 123.839)}{(1 + e^{((\phi - 0.76)/0.1)})} \quad (9)$$

5. CONCLUSIONS

The computational predictions from this study show that the epoxy mass density, volumetric shrinkage, stiffness, strength, and Poisson's ratio are strongly affected by the cross-link density. The predictions generally agree with the experimental measurements performed herein as well as those from the literature. Therefore, the computational simulation protocols are effective, and IFF-R is reliably predicting accurate physical and mechanical properties. The predicted properties at varying cross-linking densities provide insight into the evolution of properties of the epoxy system during the processing of composite materials. These data can be used as input into higher length-scale computational tools to predict the residual stresses that are developed during the processing of these complex networked epoxies in the presence of various composite reinforcements. Such modeling can be used to optimize processing parameters and improve composite laminate strength and reduce post-manufacturing residual deformations.

■ ASSOCIATED CONTENT

Supporting Information

The Supporting Information is available free of charge at https://pubs.acs.org/doi/10.1021/acsapm.1c01024.

Total energy terms in IFF-R and ReaxFF force fields; description of the comparison of sequential and nonsequential cross-linking strategies based on mass density, post-gelation volumetric shrinkage, and bulk modulus; plots of experimentally measured post-gelation volumetric shrinkage; and equations implemented in this work for mechanical property predictions using MD simulations (PDF)

Video showing the covalent bond breaking and formation between two DGEBF monomers and one DETDA hardener (MP4)

■ AUTHOR INFORMATION

Corresponding Author

Gregory M. Odegard − *Michigan Technological University, Houghton, Michigan 49931, United States;* orcid.org/0000-0001-7577-6565; Email: gmodegar@mtu.edu

Authors

Sagar Umesh Patil − *Michigan Technological University, Houghton, Michigan 49931, United States;* orcid.org/0000-0003-4301-777X

Sagar P. Shah − *University of Massachusetts, Lowell, Massachusetts 01854, United States;* orcid.org/0000-0001-6276-8435

Michael Olaya − *University of Massachusetts, Lowell, Massachusetts 01854, United States;* orcid.org/0000-0001-9710-6618

Prathamesh Prashant Deshpande − *Michigan Technological University, Houghton, Michigan 49931, United States;* orcid.org/0000-0003-1441-678X

Marianna Maiaru − *University of Massachusetts, Lowell, Massachusetts 01854, United States*

Complete contact information is available at: https://pubs.acs.org/10.1021/acsapm.1c01024

Notes

The authors declare no competing financial interest.

The raw/processed data required to reproduce these findings cannot be shared at this time as the data also form part of an ongoing study.

■ ACKNOWLEDGMENTS

This research was partially supported by the NASA Space Technology Research Institute (STRI) for Ultra-Strong Composites by Computational Design (US-COMP), grant NNX17AJ32G, and by NASA grant 80NSSC19K1246. SUPERIOR, a high-performance computing cluster at Michigan Technological University, was used in obtaining the MD simulation results presented in this publication.

REFERENCES

(1) Jin, F.-L.; Li, X.; Park, S.-J. Synthesis and application of epoxy resins: A review. *J. Ind. Eng. Chem.* **2015**, *29*, 1−11.

(2) Brostow, W.; Goodman, S. H.; Wahrmund, J. Epoxies. In *Handbook of Thermoset Plastics*, 3rd ed.; Dodiuk, H., Goodman, S. H., Eds.; William Andrew Publishing: Boston, MA, 2014; pp 191−252.

(3) Li, C.; Strachan, A. Molecular scale simulations on thermoset polymers: A review. *J. Polym. Sci., Part B: Polym. Phys.* **2015**, *53* (2), 103−122.

(4) Gartner, T. E.; Jayaraman, A. Modeling and Simulations of Polymers: A Roadmap. *Macromolecules* **2019**, *52* (3), 755−786.

(5) Patil, S. U.; Radue, M. S.; Pisani, W. A.; Deshpande, P.; Xu, H.; Al Mahmud, H.; Dumitrica, T.; Odegard, G. M. Interfacial characteristics between flattened CNT stacks and polyimides: A molecular dynamics study. *Comput. Mater. Sci.* **2020**, *185*, 109970.

(6) Pisani, W. A.; Radue, M. S.; Patil, S. U.; Odegard, G. M. Interfacial modeling of flattened CNT composites with cyanate ester and PEEK polymers. *Composites, Part B* **2021**, *211*, 108672.

(7) Bandyopadhyay, A.; Valavala, P. K.; Clancy, T. C.; Wise, K. E.; Odegard, G. M. Molecular modeling of crosslinked epoxy polymers: The effect of crosslink density on thermomechanical properties. *Polymer* **2011**, *52* (11), 2445−2452.

(8) Hadden, C. M.; Jensen, B. D.; Bandyopadhyay, A.; Odegard, G. M.; Koo, A.; Liang, R. Molecular modeling of EPON-862/graphite composites: Interfacial characteristics for multiple crosslink densities. *Compos. Sci. Technol.* **2013**, *76*, 92−99.

(9) Tack, J. L.; Ford, D. M. Thermodynamic and mechanical properties of epoxy resin DGEBF crosslinked with DETDA by molecular dynamics. *J. Mol. Graphics Modell.* **2008**, *26* (8), 1269−1275.

(10) Varshney, V.; Patnaik, S. S.; Roy, A. K.; Farmer, B. L. A Molecular Dynamics Study of Epoxy-Based Networks: Cross-Linking Procedure and Prediction of Molecular and Material Properties. *Macromolecules* **2008**, *41* (18), 6837−6842.

(11) Sundararaghavan, V.; Kumar, A. Molecular dynamics simulations of compressive yielding in cross-linked epoxies in the context of Argon theory. *Int. J. Plast.* **2013**, *47*, 111−125.

(12) Park, H.; Kim, B.; Choi, J.; Cho, M. Influences of the molecular structures of curing agents on the inelastic-deformation mechanisms in highly-crosslinked epoxy polymers. *Polymer* **2018**, *136*, 128−142.

(13) Li, C.; Strachan, A. Molecular simulations of crosslinking process of thermosetting polymers. *Polymer* **2010**, *51* (25), 6058−6070.

(14) Li, C.; Strachan, A. Molecular dynamics predictions of thermal and mechanical properties of thermoset polymer EPON862/DETDA. *Polymer* **2011**, *52* (13), 2920−2928.

(15) Li, C.; Strachan, A. Evolution of network topology of bifunctional epoxy thermosets during cure and its relationship to thermo-mechanical properties: A molecular dynamics study. *Polymer* **2015**, *75*, 151−160.

(16) Kallivokas, S. V.; Sgouros, A. P.; Theodorou, D. N. Molecular dynamics simulations of EPON-862/DETDA epoxy networks: structure, topology, elastic constants, and local dynamics. *Soft Matter* **2019**, *15* (4), 721−733.

(17) Kravchenko, O. G.; Li, C.; Strachan, A.; Kravchenko, S. G.; Pipes, R. B. Prediction of the chemical and thermal shrinkage in a thermoset polymer. *Composites, Part A* **2014**, *66*, 35−43.

(18) Sun, Y.; Chen, L.; Cui, L.; Zhang, Y.; Du, X. Molecular dynamics simulation of cross-linked epoxy resin and its interaction energy with graphene under two typical force fields. *Comput. Mater. Sci.* **2018**, *143*, 240−247.

(19) Gou, J.; Fan, B.; Song, G.; Khan, A. STUDY OF AFFINITIES BETWEEN SINGLE-WALLED NANOTUBE AND EPOXY RESIN USING MOLECULAR DYNAMICS SIMULATION. *Int. J. Nanosci.* **2006**, *05* (01), 131−144.

(20) Shenogina, N. B.; Tsige, M.; Patnaik, S. S.; Mukhopadhyay, S. M. Molecular modeling of elastic properties of thermosetting polymers using a dynamic deformation approach. *Polymer* **2013**, *54* (13), 3370−3376.

(21) Shenogina, N. B.; Tsige, M.; Patnaik, S. S.; Mukhopadhyay, S. M. Molecular Modeling Approach to Prediction of Thermo-Mechanical Behavior of Thermoset Polymer Networks. *Macromolecules* **2012**, *45* (12), 5307−5315.

(22) Jeyranpour, F.; Alahyarizadeh, G.; Arab, B. Comparative investigation of thermal and mechanical properties of cross-linked epoxy polymers with different curing agents by molecular dynamics simulation. *J. Mol. Graphics Modell.* **2015**, *62*, 157−164.

(23) Lin, P.-H.; Khare, R. Molecular Simulation of Cross-Linked Epoxy and Epoxy-POSS Nanocomposite. *Macromolecules* **2009**, *42* (12), 4319−4327.

(24) Schichtel, J. J.; Chattopadhyay, A. Modeling thermoset polymers using an improved molecular dynamics crosslinking methodology. *Comput. Mater. Sci.* **2020**, *174*, 109469.

(25) Vashisth, A.; Ashraf, C.; Zhang, W.; Bakis, C. E.; van Duin, A. C. T. Accelerated ReaxFF Simulations for Describing the Reactive Cross-Linking of Polymers. *J. Phys. Chem. A* **2018**, *122* (32), 6633−6642.

(26) Radue, M. S.; Jensen, B. D.; Gowtham, S.; Klimek-McDonald, D. R.; King, J. A.; Odegard, G. M. Comparing the Mechanical Response of Di-, Tri-, and Tetra-functional Resin Epoxies with Reactive Molecular Dynamics. *J. Polym. Sci., Part B: Polym. Phys.* **2018**, *56* (3), 255−264.

(27) Odegard, G. M.; Jensen, B. D.; Gowtham, S.; Wu, J.; He, J.; Zhang, Z. Predicting mechanical response of crosslinked epoxy using ReaxFF. *Chem. Phys. Lett.* **2014**, *591*, 175−178.

(28) Winetrout, J. J.; Kanhaiya, K.; Sachdeva, G.; Pandey, R.; Damirchi, B.; van Duin, A.; Odegard, G. M.; Heinz, H. Implementing Reactivity in Molecular Dynamics Simulations with the Interface Force Field (IFF-R) and Other Harmonic Force Fields. *arXiv/cond-mat.mtrl-sci* **2021**.

(29) Heinz, H.; Lin, T.-J.; Kishore Mishra, R.; Emami, F. S. Thermodynamically Consistent Force Fields for the Assembly of Inorganic, Organic, and Biological Nanostructures: The INTERFACE Force Field. *Langmuir* **2013**, *29* (6), 1754−1765.

(30) Pisani, W. A.; Wedgeworth, D. N.; Roth, M. R.; Newman, J. K.; Shukla, M. K. Computational Prediction of Mechanical Properties of PA6−Graphene/Carbon Nanotube Nanocomposites. *J. Phys. Chem. C* **2021**, *125* (28), 15569−15578.

(31) Odegard, G. M.; Patil, S. U.; Deshpande, P. P.; Kanhaiya, K.; Winetrout, J. J.; Heinz, H.; Shah, S. S.; Maiaru, M. Molecular Dynamics Modeling of Epoxy Resins using the Reactive Interface Force Field. *arXiv/cond-mat.mtrl-sci* **2021**.

(32) Shah, S.; Patil, S.; Deshpande, P.; Kashmari, K.; Odegard, G.; Maiaru, M. Multiscale modeling of thermoset composite to predict process-induced residual stresses. *ICCM22 2019*; Engineers Australia: Melbourne, Australia, 2019; pp 2732−2740.

(33) Shah, S.; Patil, S.; Deshpande, P.; Krieg, A.; Kashmari, K.; Mahmud, H. A.; King, J.; Odegard, G. M.; Maiaru, M. Multiscale Modeling for Virtual Manufacturing of Thermoset Composites. *AIAA Scitech 2020 Forum* **2020**, 1 DOI: 10.2514/6.2020-0882.

(34) Shah, S. P.; Maiarù, M. Effect of Manufacturing on the Transverse Response of Polymer Matrix Composites. *Polymers* **2021**, *13* (15), 2491.

(35) Patil, S. U.; Shah, S. P.; Deshpande, P. P.; Kashmari, K.; Odegard, G. M.; Maiaru, M. Prediction Of Residual Stress Build-Up In Polymer Matrix Composite During Cure Using A Two-Scale Approach. *Proceedings of the American Society for Composites−Thirty-fourth Technical Conference*, 2019.

(36) Patil, S. U.; Shah, S. P.; Deshpande, P. P.; Kashmari, K.; Olaya, M. N., Odegard, G. M.; Maiaru, M. Multi-scale Approach to Predict Cure-Induced Residual Stresses in an Epoxy System, *Proceedings of the American Society for Composites−Thirty-fifth Technical Conference, Virtual*, 2020.

(37) Deshpande, P. P.; Shah, S. P.; Patil, S. U.; Kashmari, K.; Olaya, M. N.; Odegard, G. M.; Maiarù, M. Multiscale Modelling of the Cure Process in Thermoset Polymers using ICME. *Proceedings of the American Society for Composites—Thirty-fifth Technical Conference, Virtual*, 2020.

https://doi.org/10.1021/acsapm.1c01024
ACS Appl. Polym. Mater. 2021, 3, 5788−5797

(38) Plimpton, S. Fast Parallel Algorithms for Short-Range Molecular Dynamics. *J. Comput. Phys.* **1995**, *117* (1), 1−19.
(39) Nosé, S. A molecular dynamics method for simulations in the canonical ensemble. *Mol. Phys.* **1984**, *52* (2), 255−268.
(40) Nosé, S. A unified formulation of the constant temperature molecular dynamics methods. *J. Chem. Phys.* **1984**, *81* (1), 511−519.
(41) Hoover, W. G. Canonical dynamics: Equilibrium phase-space distributions. *Phys. Rev. A: At., Mol., Opt. Phys.* **1985**, *31* (3), 1695−1697.
(42) Radue, M. S.; Jensen, B. D.; Gowtham, S.; Klimek-McDonald, D. R.; King, J. A.; Odegard, G. M. Comparing the mechanical response of di-, tri-, and tetra-functional resin epoxies with reactive molecular dynamics. *J. Polym. Sci., Part B: Polym. Phys.* **2018**, *56* (3), 255−264.
(43) Gissinger, J. R.; Jensen, B. D.; Wise, K. E. Modeling chemical reactions in classical molecular dynamics simulations. *Polymer* **2017**, *128*, 211−217.
(44) Stukowski, A. Visualization and analysis of atomistic simulation data with OVITO−the Open Visualization Tool. *Modell. Simul. Mater. Sci. Eng.* **2010**, *18* (1), 015012.
(45) Flory, P. J. *Principles of Polymer Chemistry*; Cornell University Press: Ithaca, NY, 1953.
(46) Yang, S.; Qu, J. Computing thermomechanical properties of crosslinked epoxy by molecular dynamic simulations. *Polymer* **2012**, *53* (21), 4806−4817.
(47) Estridge, C. E. The effects of competitive primary and secondary amine reactivity on the structural evolution and properties of an epoxy thermoset resin during cure: A molecular dynamics study. *Polymer* **2018**, *141*, 12−20.
(48) Malvern, L. E. *Introduction to the Mechanics of a Continuous Medium*; Prentice-Hall: Englewood Cliffs, NJ, 1969.
(49) Blaber, J.; Adair, B.; Antoniou, A. Ncorr: Open-Source 2D Digital Image Correlation Matlab Software. *Exp. Mech.* **2015**, *55* (6), 1105−1122.
(50) Harilal, R.; Ramji, M. Adaptation of Open Source 2D DIC Software Ncorr for Solid Mechanics Applications. *9th International Symposium on Advanced Science and Technology in Experimental Mechanics*, 2014.
(51) O'Brien, D. J.; White, S. R. Cure kinetics, gelation, and glass transition of a bisphenol F epoxide. *Polym. Eng. Sci.* **2003**, *43* (4), 863−874.
(52) Olaya, M. N.; Odegard, G. M.; Maiaru, M. A Novel Approach to Characterization of Composite Polymer Matrix Materials for Integrated Computational Materials Engineering Approaches. *AIAA Scitech 2021 Forum* **2021**, 1 DOI: 10.2514/6.2021-1889.
(53) Standard Test Method for Tensile Properties of Plastics.
(54) OriginLab Corporation. *OriginPro*, Version 2020b.
(55) Klimek-McDonald, D. R.; King, J. A.; Miskioglu, I.; Pineda, E. J.; Odegard, G. M. Determination and Modeling of Mechanical Properties for Graphene Nanoplatelet/Epoxy Composites. *Polym. Compos.* **2018**, *39* (6), 1845−1851.
(56) King, J. A.; Klimek, D. R.; Miskioglu, I.; Odegard, G. M. Mechanical properties of graphene nanoplatelet/epoxy composites. *J. Compos. Mater.* **2015**, *49* (6), 659−668.
(57) *Miller-Stephenson.com Product Bulletin*; pp 1−11.
(58) Littell, J. D.; Ruggeri, C. R.; Goldberg, R. K.; Roberts, G. D.; Arnold, W. A.; Binienda, W. K. Measurement of Epoxy Resin Tension, Compression, and Shear Stress–Strain Curves over a Wide Range of Strain Rates Using Small Test Specimens. *Journal of Aerospace Engineering* **2008**, *21* (3), 162−173.
(59) Gilat, A.; Goldberg, R. K.; Roberts, G. D. Strain Rate Sensitivity of Epoxy Resin in Tensile and Shear Loading. *Journal of Aerospace Engineering* **2007**, *20* (2), 75−89.

https://doi.org/10.1021/acsapm.1c01024
ACS Appl. Polym. Mater. 2021, 3, 5788−5797